Pattern formation and instability of smectic-*A* filaments grown from an isotropic phase

Hiroyoshi Naito,[1] Masahiro Okuda,[1] and Ou-Yang Zhong-can[2]
[1]*Department of Physics and Electronics, Osaka Prefecture University, Sakai, Osaka 593, Japan*
[2]*Institute of Theoretical Physics, Academia Sinica, P.O. Box 2735, Beijing 100080, China*
(Received 16 October 1996)

Pattern formation and instability of smectic-*A* filaments grown from an isotropic phase have been investigated. The evolution and shape equations for the filaments are derived by a variation of the free energy of the filaments. It is shown from the evolution equation that the length of the filament increases exponentially with time under a cooling process. It is also shown from the shape equation that the existence of the threshold length of the straight filaments for buckling and the global properties of the filaments can be predicted. The theoretical results are demonstrated experimentally in the binary mixture of octyloxycyanobiphenyl with dodecyl alcohol. [S1063-651X(97)15102-9]

PACS number(s): 61.30.Cz, 02.40.Hw, 46.30.−i, 82.65.−i

Smectic-*A* liquid crystals (Sm-*A* LC's) appear in a variety of shapes on cooling the high temperature isotropic (*I*) liquid phase [1]. The shapes have a very complex topology, and exhibit a great deal of thermotemporal evolution. Such self-organizing processes in the Sm-*A* phase are intriguing, and therefore have attracted a number of studies [2–8]. The most interesting example of the processes is the formation of Sm-*A* filament structures and their thermotemporal evolution [2,5,7]. The Sm-*A* phase first appears in the form of filaments in various Sm-*A* LC's as the *I* liquid is cooled below the *I*–Sm-*A* transition temperature [2–5,7,8]. The filaments grow rapidly in length but not in diameter. During growth, the filaments continuously buckle to take on a serpentine form, and subsequently become extremely convoluted and nearly space filling. The filaments are metastable, and eventually transform to compact domains [7].

Most of the general features of the growth of Sm-*A* nuclei are much different from those of the solidification of condensed matter such as snowflakes and ice crystals [9]. Thus studies of the formation of Sm-*A* filament structures and their thermotemporal evolution are very important for understanding pattern formation and instability in soft matter or complex fluid.

We have developed a theory for equilibrium shapes of Sm-*A* nuclei grown from the *I* phase [6,7]. Within the framework of our theory, a filamentary structure is regarded as a Sm-*A* tube with thickness of $\rho_o-\rho_i$, where ρ_o and ρ_i are the outer and inner radii of the tube, respectively. Since the Sm-*A* phase exhibits a layer structure in which the average molecular orientation is parallel to the layer normal, the filaments consist of concentric cylindrical Sm-*A* layers [2,5,6]. In this paper, we propose dynamical and static theories for a description of the dynamics and shapes of Sm-*A* filaments grown from the *I* phase. The evolution and shape equations are derived from a variation of the free energy of the filaments under cooling processes, and the growth behavior of the filaments is predicted. The predicted results are compared with the experimental results in the binary mixture of octyloxycyanobiphenyl (8OCB) with dodecyl alcohol (DODA).

The LC material used here was the binary mixture of 8OCB and DODA, whose phase diagram was reported by Pratibha and Madhusudana [5]. In this system, the nematic phase is suppressed for a molar concentration ($>20\%$) of DODA, and the *I* and Sm-*A* phases coexist in a fairly wide temperature range (for example, 42–30 °C for 60% of DODA studied here). The LC cells of dimensions 10×10 mm^2 and of thickness 50 μm bounded by glass plates were prepared. The surface of the glass plates was not treated (the observed growth pattern was not affected by the rubbing of the plates). The sample temperature was controlled in a hot stage (Mettler FP82HT) with a processor (Mettler FP90). The growth processes and the equilibrium shapes were observed with a polarizing microscope (Nikon) equipped with a charge-coupled-device video camera (Sony DXC-151A). The images were recorded and fed into an image processor (Shimadzu Nexus600).

The cells with 40% of 8OCB were cooled from the *I* phase at -0.1 °C/min, and the cooling was stopped at 36.4 °C in the coexisting region for the observation of equilibrium Sm-*A* shapes. Figure 1 shows the initial stage of the growth sequence of a Sm-*A* filament from *I* phase in the mixture of 8OCB and DODA at a cooling rate of -0.1 °C/min. As stated above, the filament finally collapses forming compact domains at the LC/glass interfaces [7]. We have reported that the compact domains have toroidal structures with a ratio of generating radii of $1/\sqrt{2}\sim1$ [7], but in rare cases a circular (toroidal) filament whose ring width is almost equal to the diameter of the straight filaments is found. Figure 2 shows an equilibrium circular Sm-*A* filament grown from an *I* phase observed at 36.4 °C.

A Sm-*A* filament of length *l* can be described by a tube with the outer and inner surfaces,

$$\vec{r}_o=\vec{r}(s)+\rho_o(\vec{n}\cos\nu+\vec{b}\sin\nu),$$
$$\vec{r}_i=\vec{r}(s)+\rho_i(\vec{n}\cos\nu+\vec{b}\sin\nu), \tag{1}$$

respectively, where $0\leqslant s\leqslant l$, $0\leqslant\nu\leqslant2\pi$, $\vec{r}$ is the axial curve of the filament, and $\vec{n}(s)$ and $\vec{b}(s)$ are the normal and binormal vectors of $\vec{r}$, respectively [10] (from the experimental results in Fig. 1, it is reasonable to assume that the radii ρ_o

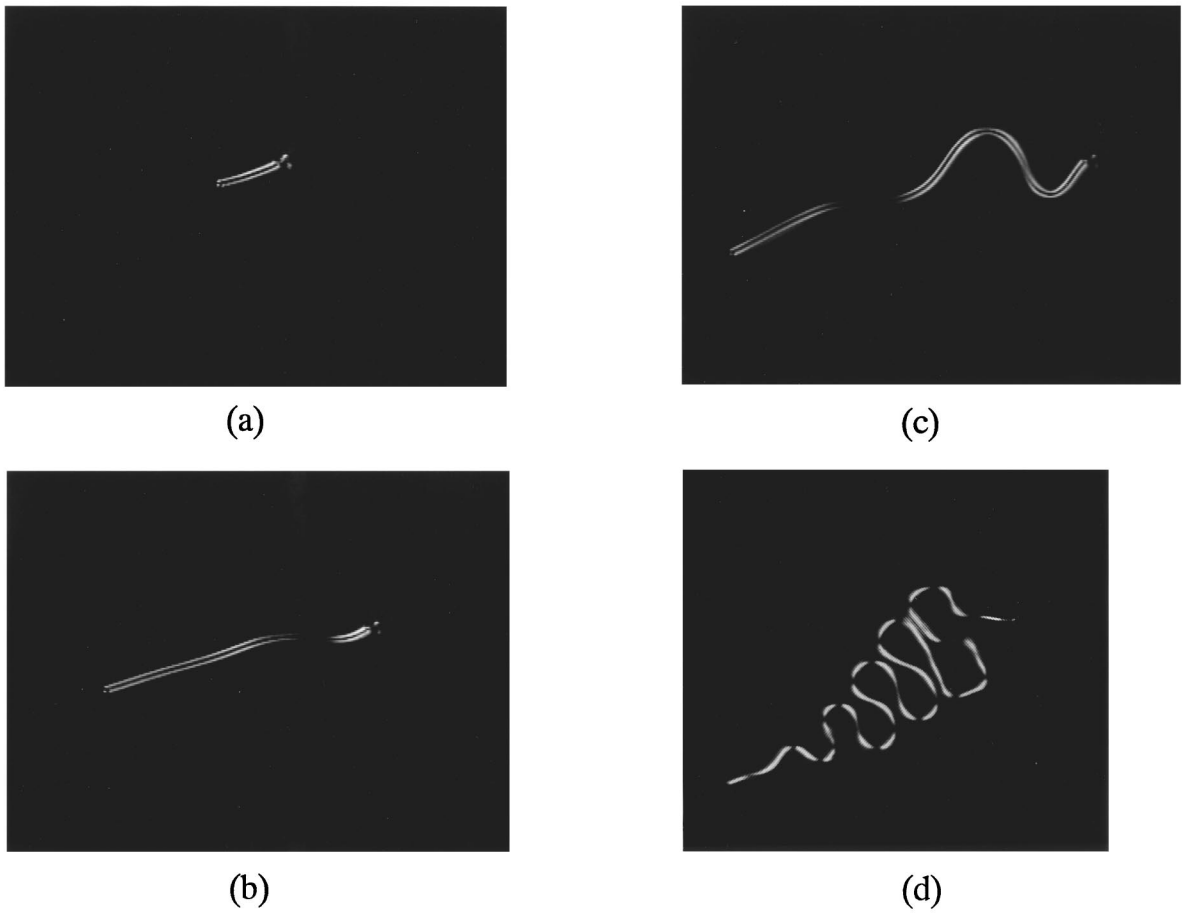

FIG. 1. Growth sequence of a Sm-*A* filament from the *I* phase in the mixture of 8OCB and DODA (the molar concentration of 8OCB is 40%) at a cooling rate of −0.1 °C/min. (a)–(c) and (d) are about 166 and 500 μm wide, respectively.

and ρ_i are constant throughout the filament during the growth). As we have shown in Ref. [6], the net difference in the energy between Sm-*A* and *I* phases is the sum of the following three terms: (1) the volume free energy change due to *I*–Sm-*A* transition $F_V=-g_oV$, where g_o is the difference in the Gibbs free energy densities between *I* and Sm-*A* phases, and *V* is the volume of the Sm-*A* nucleus; (2) the surface energy of the outer and inner Sm-*A*–*I* interfaces $F_A=\gamma(A_o+A_i)$, where γ is the Sm-*A*–*I* interfacial tension, and A_o and A_i are the surface areas of the outer and inner surfaces, respectively; and (3) the curvature elastic energy of the Sm-*A* filament $F_C=(k_{11}/2)\int(\vec{\nabla}\cdot\vec{N})^2dV+(2k_{11}+k_5)(\rho_o-\rho_i)\oint KdA_i$, where $\vec{N}$ is the director, *K* is the Gaussian curvature defined on the inner surface, and $k_5=2k_{13}-k_{22}-k_{24}$ (k_{ij} the Oseen-Frank elastic constants [11]). By assuming that ρ_o and ρ_i are small, so that $\|\rho_o k(s)\|\ll 1$, where $k(s)$ is the curvature of $\vec{r}(s)$, the energy for the Sm-*A* filament grown from the *I* phase is then represented as a line integration,

FIG. 2. Circular Sm-*A* filament grown from the *I* phase in the mixture of 8OCB and DODA (the molar concentration of 8OCB is 40%) observed at 36.4 °C. The picture is about 166 μm wide.

$$F=-\pi(\rho_o^2-\rho_i^2)\int g_o ds+2\pi(\rho_o+\rho_i)\gamma\int ds+\pi k_{11}\int\left[\ln\left(\frac{\rho_o}{\rho_i}\right)+\ln\left(\frac{1+\sqrt{1-k^2\rho_i^2}}{1+\sqrt{1-k^2\rho_o^2}}\right)\right]ds, \quad (2)$$

where the term $(2k_{11}+k_5)(\rho_o-\rho_i)\oint KdA_i$ in F_C was omitted because the term is constant according to the Gauss-Bonnet theorem [10]. Since the temperature gradient along a long Sm-*A* filament is expected to exist, g_o in Eq. (2) is dependent on *s* [12]. On the other hand, γ is not dependent on *s*, because γ exhibits no temperature dependence or a weak one [5].

The major difference in the growth processes between solids and Sm-A filaments is that growth of solids is observed at solid-liquid interfaces, while the filaments grow in length but not in diameter. For this reason, the length s and axial curve $\vec{r}(s)$ of a Sm-A filament should be considered as $\vec{r}(s,t)$ during the growth of the filament, and hence the normal and binormal vectors should also be $\vec{n}(s,t)$ and $\vec{b}(s,t)$, respectively. Thus the problem we are interested in here is how to express the evolution equation of the filaments in terms of $\vec{r}(s,t)$.

To do this, we introduce a time-independent parameter u in order to replace the arc length s with u. Then $\vec{r}(u,t)$ $[=\vec{r}(s,t)]$ can be seen as a one-dimensional (1D) ''surface,'' and thereby we have the first fundamental form of the surface, $ds=\sqrt{g}du$, where $g=\vec{r}_u\cdot\vec{r}_u$ and $\vec{r}_u=\partial_u\vec{r}$. The curvature of $\vec{r}(u,t)$ is expressed as $k(s)^2=\vec{r}_{ss}\cdot\vec{r}_{ss}=g^{-2}(\vec{r}_{uu}\cdot\vec{r}_{uu})-g^{-3}(\vec{r}_{uu}\cdot\vec{r}_u)$, where $\vec{r}_{ss}=\partial_s^2\vec{r}$ and $\vec{r}_{uu}=\partial_u^2\vec{r}$. Since $\|\rho_o k(s)\|\ll 1$ and $\|\rho_1 k(s)\|\ll 1$, we can rewrite $\ln[(1+\sqrt{1-k^2\rho_i^2})/(1+\sqrt{1-k^2\rho_o^2})]$ in Eq. (2) as $(\rho_o^2-\rho_i^2)k^2/4$. Then, Eq. (2) becomes the Helfrich energy in 1D membranes [11],

$$F=k_c\int k(s)^2ds+\lambda\int ds+\int \sqcap(s)ds, \tag{3}$$

where $k_c=\pi k_{11}(\rho_o^2-\rho_i^2)/4$ is the 1D bending rigidity, $\lambda=\pi k_{11}\ln(\rho_o/\rho_i)+2\pi\gamma(\rho_o+\rho_i)$ is the 1D tension, and $\sqcap=-\pi g_o(\rho_o^2-\rho_i^2)$ is the 1D potential.

The Sm-A phase grows from the I phase in a diffusion field of temperature T, which satisfies

$$D\vec{\nabla}^2T=\partial_tT, \tag{4}$$

where D is the thermal diffusion constant (the difference in D between Sm-A and I phases is neglected [9]). Since g_o can be related to T via $g_o=\Delta H(T_c-T)/T_cv_m$ [12], where ΔH is the transformation enthalpy, T_c is the I–Sm-A transformation temperature, and v_m is the molar volume of Sm-A LC, we treat $\sqcap$ as a potential. The energy conservation at the arc element ds along the Sm-A filament can be expressed as $\partial_t dF=-k^*\oint\vec{\nabla}T\cdot d\vec{A}$, where $dF=(k_ck^2+\lambda+\sqcap)ds$, $k^*=Dc_p$, c_p is the specific heat of the LC, and the surface integral is carried out over the surface of the element. Using the Gauss theorem, $\oint\vec{\nabla}T\cdot d\vec{A}=\int\vec{\nabla}^2Tdv=\vec{\nabla}^2T\pi(\rho_o^2-\rho_i^2)ds$, and Eq. (4), we have

$$\overline{c_p}\partial_tT=-\frac{1}{\sqrt{g}}\partial_t[\sqrt{g}(k_ck^2+\lambda+\sqcap)], \tag{5}$$

where $\overline{c_p}=\pi(\rho_o^2-\rho_i^2)c_p$ is 1D specific heat of the Sm-A filament (i.e., the specific heat per unit length of the filament). This is the evolution equation that governs the growth velocity of the filament. In the case of a straight Sm-A filament [$\vec{r}=q(t)u\vec{a}_o$, where $\vec{a}_o$ is the unit vector of the growth direction and $q(t)$ corresponds to the growth of the length of the filament] at a spatially uniform constant cooling rate R $(dT/dt=-R)$, we obtain $q(t)=q(0)\exp(\alpha t)$ from Eq. (5),

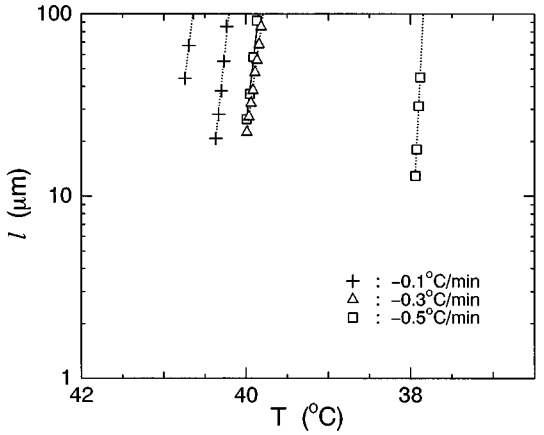

FIG. 3. Length of Sm-A filaments grown from the I phase as a function of temperature at several cooling rates in the mixture of 8OCB and DODA (the molar concentration of 8OCB is 40%).

where $\alpha=\overline{c_p}R/(\lambda+\sqcap)$. The straight filaments can be observed in the early stage of the growth as shown in Fig. 1(a). Such an exponential behavior was explained in terms of a different model, based on the flow of solidification current through the filament surface [2,5], while our present explanation is based on the flow of heat current. To show the validity of the present theory, we experimentally examined the temperature dependence of ℓ of the straight filaments at several cooling rates (Fig. 3), because the theory predicts that $d\ln\ell/(-dT)$ is calculated to be $\overline{c_p}/(\lambda+\sqcap)$, and hence $d\ln\ell/(-dT)$ is independent of R. In Fig. 3, we can see that all the lines on the $\ln\ell$ vs T plot are straight, and that the slopes of these lines are almost the same (independent of R), yielding the validity of the theoretical predictions.

Growth shapes of Sm-A filaments in 3D cannot be determined by the evolution equation (5) alone. To determine the shapes, two more equations, which we will show below, are necessary. We consider a slightly distorted curve $\vec{r}'$ from $\vec{r}$, $\vec{r}'=\vec{r}+\varphi(u)\vec{n}+\psi(u)\vec{b}$, where $\varphi(u)$ and $\psi(u)$ are sufficiently small and smooth functions. Using the Frenet formulas [10]

$$\vec{r}_{ss}=k(s)\vec{n},$$

$$\vec{n}_s=-k(s)\vec{r}_s-\tau(s)\vec{b}, \tag{6}$$

$$\vec{b}_s=\tau(s)\vec{n},$$

where $\vec{n}_s=\partial_s\vec{n}$, $\vec{b}_s=\partial_s\vec{b}$, and $\tau(s)$ is the torsion of $\vec{r}$, we have derived the change in the free energy due to the distortion from Eq. (3) [13],

$$\delta F=\int\{\varphi[-(\sqcap+\lambda)k+k_c(2k_{ss}+k^3-2\tau^2k)+\beta\vec{n}\cdot\vec{\nabla}T]$$
$$+\psi[k_c(-2k_s\tau-k\tau_s)+\beta\vec{b}\cdot\vec{\nabla}T]\}ds, \tag{7}$$

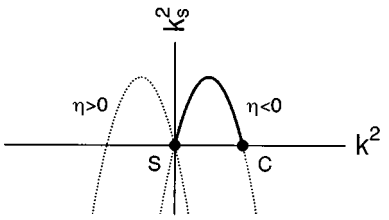

FIG. 4. Phase diagram of Sm-*A* filaments displayed on a plot of k_s^2 vs k^2. Points *S* and *C* represent straight filaments and circular filaments, respectively.

where $\beta=-\sqcap/(T_c-T)=\pi(\rho_o^2-\rho_i^2)\Delta H/T_c v_m$, $k_s=\partial_s k$, $k_{ss}=\partial_s^2 k$, and $\tau_s=\partial_s\tau$. The equilibrium shapes of Sm-*A* filaments are obtained from $\delta F=0$, which leads to the following two conditions:

$$-(\sqcap+\lambda)k+k_c(2k_{ss}+k^3-2\tau^2 k)+\beta\vec{n}\cdot\vec{\nabla}T=0, \quad (8)$$

$$k_c(-4k_s\tau-2k\tau_s)+\beta\vec{b}\cdot\vec{\nabla}T=0. \quad (9)$$

These shape equations represent the balance of normal forces per unit arc length of the filament. It is obvious that a straight filament $\vec{r}=q(t)u\vec{a}_o$ is a solution of Eqs. (8) and (9) if the normal and binormal vectors satisfy $\vec{n}\cdot\vec{\nabla}T=0$ and $\vec{b}\cdot\vec{\nabla}T=0$. These conditions are satisfied when the temperature is spatially uniform or $\vec{a}_o$ is parallel to $\vec{\nabla}T$ ($\vec{a}_o\|\vec{\nabla}T$ means that the straight filament develops along $-\vec{\nabla}T$ [13], which is consistent with physical processes of solidification [9]).

It can be seen from Fig. 1 that after the length of the filaments attains a certain critical length, the straight filaments begin to buckle. Such symmetry breaking is the most important feature in pattern formation processes. To understand this, we try to solve Eqs. (8) and (9) in the case of plane curves, which are consistent with the 2D geometry of Sm-*A* filaments observed in experiments [2,5,7]. For a plane curve on the *x*-*y* plane, the Frenet formulas Eq. (6) give $\tau=0$ and a $\vec{b}\|z$ axis. Substituting $\tau=0$ into Eq. (9), we obtain $\vec{z}\cdot\vec{\nabla}T=0$, where $\vec{z}$ is the unit vector in the *z* direction. In what follows, we consider the case where *T* is spatially uniform for simplicity. Then Eq. (8) is rewritten as

$$-(\sqcap+\lambda)k(s)+k_c(2k_{ss}+k^3)=0. \quad (10)$$

Its first integration is $k_s^2=C_1-\eta k^2-\frac{1}{4}k^4$, where $\eta=-(\sqcap+\lambda)/2k_c$, and C_1 is the integration constant. For a plane curve having straight line portion, C_1 is zero. The first integration is thus reduced to

$$k_s^2=-k^2(\tfrac{1}{4}k^2+\eta). \quad (11)$$

We illustrate the behavior of k_s^2 as a function of k^2 in Fig. 4, where the solid curve represents physically acceptable region because of k^2, $k_s^2\geqslant 0$. It is evident from the expressions for λ and $\sqcap$ that λ increases, while $\sqcap$ decreases with decreasing temperature from the *I*–Sm-*A* transition temperature. These temperature dependences of λ and $\sqcap$ are governed mainly by those of k_{11} [1] and g_o [12], respectively. If $\lambda<\|\sqcap\|$ just below the *I*–Sm-*A* transition temperature and $\lambda>\|\sqcap\|$ well below the *I*–Sm-*A* transition temperature, the sign of η is changed from positive to negative as the temperature is lowered. On the basis of these assumptions, we see from this phase diagram that a Sm-*A* straight filament is located at $k^2=k_s^2=0$ (the point *S* in Fig. 4) on the $\eta>0$ branch in the initial stage of a cooling process. As the temperature is further decreased, the sign of η is changed from positive to negative, and hence the location of the filament moves from the point *S* to a point on the solid curve of the $\eta<0$ branch in Fig. 4, meaning that the straight filament begins to buckle. From this behavior, the length of the filament at $\eta=0$ is regarded as the threshold length for the buckling of a straight filament.

The global property of such a buckled filament can be examined from the integration of Eq. (11) for $\eta<0$, which is

$$k^2=-\frac{4\eta}{\cosh^2(\sqrt{-\eta}s)}. \quad (12)$$

From this equation, we find that k^2 tends to 0 for $s\rightarrow\pm\infty$, indicating that both ends of a buckled filament are straight. This is consistent with the experimental observation in Fig. 1(d). Note that such a feature has often been found in literature [3,14], and has been reproduced by computer simulation [2].

According to the four-vertex theorem, that states that a simple closed convex curve has at least four vertices [10], we show that a Sm-*A* filament can form a closed curve because it is obvious from Eq. (11) that the Sm-*A* filament has four vertices for $k_s=0$. Thus it is expected that some straight filaments observed in the initial stage of the growth buckle, and the ends of the filaments fuse to form closed curves. In the phase diagram, this structure corresponds to the point *C* in Fig. 4. The present prediction is confirmed experimentally as shown in Fig. 2 (similar structures have been reported [3,4,8]). The circular filament developed from a straight cylinder may be seen in the initial stage of the formation process of focal conic domain [7,8,15].

In summary, we have studied the thermotemporal evolution of Sm-*A* filaments grown from the *I* phase. We have first derived the free energy of the filaments. Then the evolution and shape equations have been derived by a variation of the free energy of the filament. We show from the evolution equation that the length of the filament increases exponentially under a cooling process. The shape equations can be analytically solved for plane curves. We also show from the analytical solution that a threshold length of the straight filaments for buckling exists, and that the global properties of the filaments characterized by open and closed curves predict a filament with both ends being straight, and a circular filament, respectively. The theoretical predictions are demonstrated experimentally in the binary mixture of 8OCB with DODA. Finally, we mention that a structural change at a molecular level such as the *trans* to *cis* transition in alkyl chains of 8OCB molecules is a possible physical origin of the buckling of the filaments, because the change may modify k_{11} and hence η in Eq. (11). This problem is of

fundamental importance for understanding of pattern formation in LC, and will be discussed in a future work.

We would like to thank Professor A. Sugimura of Osaka Sangyo University for helpful conversation, and Merck Japan Limited for supplying LC materials. This work was partially supported by Advanced Research Foundation of Osaka Prefecture University and by National Science Foundation of China.

[1] P. G. de Gennes, *The Physics of Liquid Crystals* (Clarendon, Oxford, 1975).
[2] P. Palffy-Muhoray, B. Bergersen, H. Lin, R. B. Meyer, and Z. Rácz, in *Pattern Formation in Complex Dissipative Systems*, edited by S. Kai (World Scientific, Singapore, 1992), p. 504.
[3] A. Adamczyk, Mol. Cryst. Liq. Cryst. **170**, 53 (1989); Thin Solid Films, **244**, 758 (1994).
[4] S. L. Arora, P. Palffy-Muhoray, R. A. Vora, D. J. David, and A. M. Dasgupta, Liq. Cryst. **5**, 133 (1989).
[5] R. Pratibha and N. V. Madhusudana, J. Phys. (France) II **2**, 383 (1992).
[6] H. Naito, M. Okuda, and Ou-Yang Zhong-can, Phys. Rev. Lett. **70**, 2912 (1993).
[7] H. Naito, M. Okuda, and Ou-Yang Zhong-can, Phys. Rev. E **52**, 2095 (1995).
[8] A. Adamczyk, Mol. Cryst. Liq. Cryst. **249**, 75 (1994); **261**, 271 (1995).
[9] J. S. Langer, Rev. Mod. Phys. **52**, 1 (1980).
[10] M. P. do Carmo, *Differential Geometry of Curves and Surfaces* (Prentice-Hall, Englewood Cliffs, NJ, 1976).
[11] W. Helfrich, Z. Naturforsch. **28C**, 693 (1973); Ou-Yang Zhong-can, S. Liu, and Xie Yu-zhang, Mol. Cryst. Liq. Cryst. **204**, 143 (1991).
[12] N. J. Chou, S. W. Depp, J. M. Eldrige, M. H. Lee, G. J. Sprokel, A. Juliana, and J. Brown, J. Appl. Phys. **54**, 1827 (1983).
[13] The details will be described in a future work by the current authors.
[14] N. Nawa, Jpn. J. Appl. Phys. **29**, 1521 (1990).
[15] W. Bragg, Nature **133**, 445 (1934).